Inorganic Chemistry

Article

pubs.acs.org/IC

Expansion of Antimonato Polyoxovanadates with Transition Metal Complexes: $(Co(N_3C_5H_{15})_2)_2[\{Co(N_3C_5H_{15})_2\}V_{15}Sb_6O_{42}(H_2O)]\cdot 5H_2O$ and $(Ni(N_3C_5H_{15})_2)_2[\{Ni(N_3C_5H_{15})_2\}V_{15}Sb_6O_{42}(H_2O)]\cdot 8H_2O$

Elena Antonova,[†] Christian Näther,[†] Paul Kögerler,[‡] and Wolfgang Bensch*[,†]

[†]Institut für Anorganische Chemie, Christian-Albrechts-Universität zu Kiel, D-24118 Kiel, Germany

[‡]Institut für Anorganische Chemie, RWTH Aachen Universität, D-52074 Aachen, Germany

Supporting Information

ABSTRACT: Two new polyoxovanadates $(Co(N_3C_5H_{15})_2)_2[\{Co(N_3C_5H_{15})_2\}V_{15}Sb_6O_{42}(H_2O)]\cdot 5H_2O$ (**1**) and $(Ni(N_3C_5H_{15})_2)_2[\{Ni(N_3C_5H_{15})_2\}V_{15}Sb_6O_{42}(H_2O)]\cdot 8H_2O$ (**2**) ($N_3C_5H_{15}$ = *N*-(2-aminoethyl)-1,3-propanediamine) were synthesized under solvothermal conditions and structurally characterized. In both structures the $[V_{15}Sb_6O_{42}(H_2O)]^{6-}$ shell displays the main structural motif, which is strongly related to the $\{V_{18}O_{42}\}$ archetype cluster. Both compounds crystallize in the triclinic space group $P\bar{1}$ with a = 14.3438(4), b = 16.6471(6), c = 18.9186(6) Å, α = 87.291(3)°, β = 83.340(3)°, γ = 78.890(3)°, and V = 4401.4(2) Å^3 (**1**) and a = 14.5697(13), b = 15.8523(16), c = 20.2411(18) Å, α = 86.702(11)°, β = 84.957(11)°, γ = 76.941(11)°, and V = 4533.0(7) Å^3 (**2**). In the structure of **1** the $[V_{15}Sb_6O_{42}(H_2O)]^{6-}$ cluster anion is bound to a $[Co(N_3C_5H_{15})_2]^{2+}$ complex via a terminal oxygen atom. In the Co^{2+}-centered complex, one of the amine ligands coordinates in tridentate mode and the second one in bidentate mode to form a strongly distorted CoN_5O octahedron. Similarly, in compound **2** an analogous NiN_5O complex is joined to the $[V_{15}Sb_6O_{42}(H_2O)]^{6-}$ anion via the same attachment mode. A remarkable difference between the two compounds is the orientation of the noncoordinated propylamine group leading to intermolecular Sb···O contacts in **1** and to Sb···N interactions in **2**. In the solid-state lattices of **1** and **2**, two additional $[M(N_3C_5H_{15})_2]^{2+}$ complexes act as countercations and are located between the $[\{M(N_3C_5H_{15})_2\}V_{15}Sb_6O_{42}(H_2O)]^{4-}$ anions. Between the anions and cations strong N−H···O hydrogen bonds are observed. In both compounds the clusters are stacked along the b axis in an ABAB fashion with cations and water molecules occupying the space between the clusters. Magnetic characterization demonstrates that the Ni^{2+} and Co^{2+} cations do not significantly couple with the S = 1/2 vanadyl groups. The susceptibility data can be successfully reproduced assuming a distorted ligand field for the Co^{2+} ions (**1**) and an O_h-symmetric Ni^{2+} ligand field (**2**).

1. INTRODUCTION

During the past few years the field of polyoxometalate (POM) chemistry made enormous progress because of the interesting properties and possible applications of POMs covering areas like supramolecular, analytical and clinical chemistry, as electronic and protonic conductors, in medicine, in batteries, and in sorption[1−5] to name just a few. The structural and physical properties of isopolyanions may be significantly altered by inner-core modification introducing heteroatoms in the cluster shells as observed for many antimony-containing polyoxotungstates[6−9] and polyoxomolybdates.[10−13] Compared to Mo- and W-based POM chemistry that of the lightest homologue V is much less developed and antimony substituted polyoxovanadates (POVs) are scarce. In the CSD database less than 30 antimony POVs are collected and only 10 exhibit cluster shell structures such as $[V_{14}Sb_8O_{42}]^{4-}$, $[V_{15}Sb_6O_{42}]^{6-}$, and $[V_{16}Sb_4O_{42}]^{8-}$.[14−18] This finding is surprising because antimony-based POVs exhibit interesting properties and may be applied in heterogeneous oxidation catalysis.[19] Additionally, antimony cations have a stabilizing effect on POMs at high temperatures.[20] Some further applications of antimonato POVs may be in selective oxidation reactions,[21] as deNO$_x$ catalysts,[2] or in sorption applications.[22]

Besides the chemical modification of the cluster shells of POMs the second strategy to alter the chemical and physical properties is to expand the cores by binding further building units like transition metal complexes or large aggregates to exposed oxygen sites of the cluster anions.[16,23] There are only few reports of such functionalization of antimonato POVs, namely, $[\{Co(en)_2\}_2V_{14}Sb_8O_{42}(H_2O)]\cdot 6H_2O$ by $[Co(en)_2]^{2+}$,[18] $[V_{16}Sb_4O_{42}(H_2O)\{VO(C_6H_{14}N_2)_2\}_4]\cdot 10H_2O\cdot C_6H_{14}N_2$ ($C_6H_{14}N_2$ = (±)-*trans*-1,2-diaminocyclohexane),[16] $[\{Ni(en)_2\}_2Sb_8V_{14}O_{42}]\cdot 5.5H_2O$ by $[Ni(en)_2]^{2+}$,[24] $[Zn_2(dien)_3][\{Zn(dien)\}_2V_{16}Sb_4O_{42}(H_2O)]\cdot 4H_2O$, $[Zn(dien)_2]_2$ $[\{Zn$-

Received: October 26, 2011
Published: January 10, 2012

   dx.doi.org/10.1021/ic2023117 | *Inorg. Chem.* 2012, 51, 2311−2317

$(dien)\}_2(V_{14}Sb_8O_{42})_2(H_2O)]\cdot 4H_2O$ by $[Zn(dien)_2]^{2+}$.[25] This observation is in striking difference to the arsenato POV chemistry where several expanded and interconnected $[V_{18-x}As_{2x}O_{42}]\cdot nH_2O$ (x = 2–4) clusters were reported.[26−30] Very recently we were able to functionalize $[V_{15}Sb_6O_{42}]^{6-}$ and $[V_{14}Sb_8O_{42}]^{4-}$ cluster anions with 1-(2-aminoethyl)piperazine amine molecules showing very short Sb–N distances indicative for weak bonding interactions.[31] In our ongoing work to chemically modify the shells of antimonato POV clusters we crystallized and characterized the two new compounds $(Co(N_3C_5H_{15})_2)_2[\{Co(N_3C_5H_{15})_2\}V_{15}Sb_6O_{42}(H_2O)]\cdot 5H_2O$ (**1**) and $(Ni(N_3C_5H_{15})_2)_2[\{Ni(N_3C_5H_{15})_2\}$-$V_{15}Sb_6O_{42}(H_2O)]\cdot 8H_2O$ (**2**). Here we report the synthesis and X-ray crystal structure analysis of these new antimonato POVs and their magnetic properties. The spherical $[V_{15}Sb_6O_{42}(H_2O)]^{6-}$ cluster anion in both compounds is analogous to the cluster $[V_{15}As_6O_{42}(H_2O)]^{6-}$, which has been intensively studied because of its interesting magnetic properties[32,33] and spin frustration-related phenomena.[34,35] This cluster type has been considered for applications in quantum computing owing to its unusually long spin coherence lifetime.[36]

2. RESULTS AND DISCUSSION

2.1. Crystal Structures. The new compounds **1** and **2** crystallize in the triclinic space group $P\bar{1}$ with two formula units per unit cell. Selected crystal data and details of the structure determination of compounds **1** and **2** are shown in Table 1.

Table 1. Selected Crystal Data and Details of the Structure Determination of Compound 1 and 2

	compound **1**	compound **2**
chemical formula	$C_{30}H_{102}Co_3N_{18}O_{48}Sb_6V_{15}$	$C_{30}H_{108}Ni_3N_{18}O_{51}Sb_6V_{15}$
formula weight	3154.6538	3207.9700
crystal system	triclinic	triclinic
space group	$P\bar{1}$	$P\bar{1}$
a/Å	14.3438(4)	14.5697(13)
b/Å	16.6471(6)	15.8523(16)
c/Å	18.9186(6)	20.2411(18)
α/deg	87.291(3)	86.702(11)
β/deg	83.340(3)	84.957(11)
γ/deg	78.890(3)	76.941(11)
volume/Å^3	4401.4(2)	4533.0(7)
Z	2	2
temperature/K	293	170
λ/Å	0.71073	0.71073
D_{calc}/g cm^{-3}	2.380	2.327
reflections collected	52541	38746
independent reflections	16581	16324
R(int)	0.0392	0.0406
R1 for $[I > 2\sigma(I)]$	0.0331	0.0337
GOF	1.058	0.943
wR2 for all reflections	0.0800	0.0835

The central structural motif of both compounds is the $[V_{15}Sb_6O_{42}]^{6-}$ cluster with one neutral H_2O molecule located in the center of the spherical shell. The distances between the oxygen atom of the water molecule and the V atoms of the cluster are in the range of 3.7095(1) to 3.9538(1) Å for **1** and 3.5974(4) to 4.1571(5) Å for **2**.

A simple way to derive the spherical shell of $[V_{15}Sb_6O_{42}]^{6-}$ is to substitute three VO_5 square pyramids by three Sb_2O_5 moieties from the $\{V_{18}O_{42}\}$ archetype cluster. Consequently 15 VO_5 square pyramids and 3 Sb_2O_5 handle-like moieties which are formed by corner-sharing of SbO_3 units (Sb–O bond lengths: 1.925(3)–1.968(3) Å for **1**; 1.937(4)–2.025(4) Å for **2**) construct the cluster anion (Figure 1). Two caps consisting

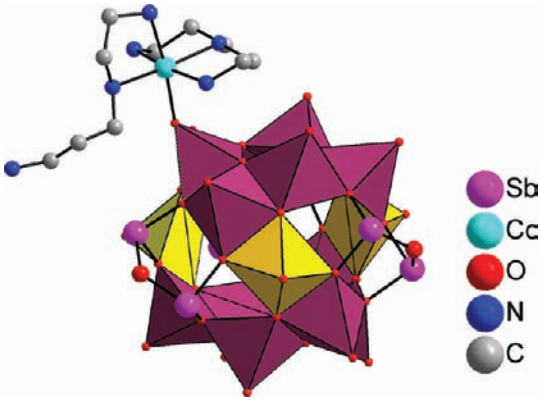

Figure 1. Central fragment of compound **1** with the Co^{2+} centered complex covalently bound to the cluster shell. H atoms are not displayed for clarity. The polyhedra highlighted in yellow represent the O=VO_4 pyramids representing the central spin-frustrated V_3 triangle.

of six edge-share VO_5 pyramids enwrap the remaining three VO_5 polyhedra also by edge-sharing. The structure of the cluster is identical with that of the well-known arsenato analogue.[25] There are two types of V–O bonds in the clusters: basal V–O (1.903(3)–2.022(3) Å for **1** and 1.906(4)–2.029(4) Å for **2**) and shorter terminal V=O (1.594(4)–1.629(3) Å for **1** and 1.607(4)–1.638(4) Å for **2**) which point outward. The shortest V···V distances are between 2.8507(10) and 3.0654(10) Å for **1** and between 2.8196(14) and 3.0767(15) Å for **2**. All geometric parameters (Supporting Information, Tables S1 and S2) are in line with those reported in literature for POVs.[14−16]

There are three crystallographically independent Co^{2+} ions (Co1, Co2, and Co3) in **1** located on general positions. Co1 is coordinated by a terminal oxygen atom of the cluster anion, three N atoms from one $N_3C_5H_{15}$ ligand, and two N donors from the ethyl moiety of the second amine molecule (Figure 1 and Figure 2, left). The resulting octahedron around Co1 is severely distorted with Co–N bonds from 2.139(4) to 2.202(4) Å and a Co–O bond of 2.111(3) Å. The trans O–Co1–N angle of 173.50(15)° and Co–N bond lengths are in agreement with data reported in literature.[37]

The remaining two Co^{2+} ions are in an octahedral environment of two tridentate $C_5H_{15}N_3$ ligands with Co–N bonds of 2.136(4)–2.225(5) Å for Co2 and of 2.156(4)–2.205(5) Å for Co3 (Figure 2, right). The bond lengths and the angles around the Co^{2+} cations clearly indicate a distortion from ideal octahedral symmetry (Supporting Information, Table S1).

The clusters are arranged in layers parallel to the (100) plane. The water solvate molecules and the two isolated Co^{2+} centered complexes occupy the free voids between these layers. Along the b axis the layers alternate in an ABAB fashion (Figure 3). In the A layers the complexes are located above the cluster anions, and in the B layers they are beneath them. Considering the Sb–O distance (3.134(3) Å; sum of van der Waals radii:

dx.doi.org/10.1021/ic2023117 | Inorg. Chem. 2012, 51, 2311–2317

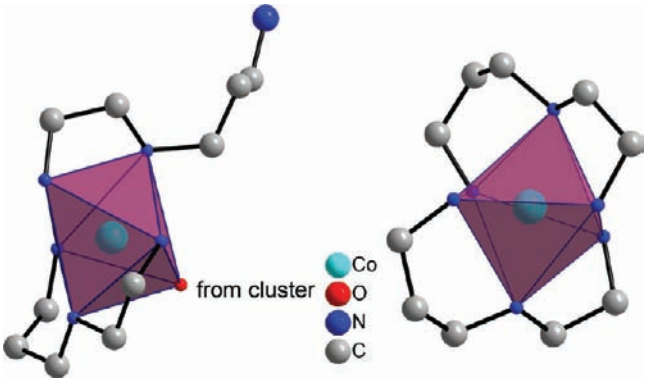

Figure 2. Representation of the transition metal complex $[Co(N_3C_5H_{15})_2]^{2+}$ with Co1 (left) and Co2 and 3 (right). H atoms are omitted for clarity.

3.52 Å) as a weak intercluster interaction, pairs of cluster anions are formed as outlined within the ellipsoidal area in Figure 3.

In total there are 29 N−H···O hydrogen bonds ranging from 2.0805(1) Å to 2.8946(1) Å, bridging water and Co^{2+} complexes as well as the Co complexes and the cluster anions in the structure. The Co1 complex is involved in 4 such interactions, whereas the Co2 complex has only 2 N−H···O contacts and the Co3 complex has 6 H bonding interactions. Hence, three different cluster anions and one water molecule are interconnected by each complex cation leading to the formation of a three-dimensional network structure.

Like in compound **1** the cluster anion in **2** is bound through a terminal oxygen atom (O1) to a transition metal complex $[Ni(N_3C_5H_{15})_2]^{2+}$ and the Ni^{2+} ion is coordinated by the O atom, three N atoms from one $C_5H_{15}N_3$ ligand and two N donors from the ethyl moiety of a second amine molecule (see Figure 1). The resulting octahedral environment is distorted with Ni2−N bond lengths of 2.101(5)−2.128(5) Å and a Ni2−O bond of 2.126(4) Å (Supporting Information, Table S2). The remaining two Ni^{2+} cations are each octahedrally coordinated by two tridentate amine molecules. The geometric parameters of the two Ni^{2+} complexes (Supporting Information, Table S2) agree well with literature data.[38,39]

An interesting feature of compound **2** is the relative short distance between Sb atoms of the cluster shells and N atoms from the propylchain of the complex $[Ni2(N_3C_5H_{15})_2]^{2+}$ of neighbored clusters (Sb−N: 2.654(5) Å). Because of these short distances "rings" are formed consisting of two $[V_{15}Sb_6O_{42}]^{6-}$ clusters (Figure 4). Short distances between Sb atoms of antimonato POV clusters and N atoms of amine molecules has been recently reported for the POVs $[V^{IV}{}_{14}Sb^{III}{}_8(C_6H_{15}N_3)_4O_{42}(H_2O)]\cdot 4H_2O$ (Sb−N: 2.528(7) and 2.536(9) Å) and $(C_6H_{17}N_3)_2[V^{IV}{}_{15}Sb^{III}{}_6(C_6H_{15}N_3)_2O_{42}(H_2O)]\cdot 2.5H_2O$ (Sb−N: 2.542(6) and 2.502(6) Å).[29] Considering the relatively short Sb−N distances between neighboring cluster anions pairs are formed like in compound **1**, where intercluster Sb···O interactions leads to the formation of such pairs.

An extended H bonding network with 28 N−H···O contacts the range from 2.0719(3) Å to 2.9947(3) Å join the constituents into a three-dimensional network structure. The Ni1 complex is involved in 7 hydrogen bonds, the Ni2 complex has 12 and the Ni3 complex has 9 such hydrogen bonding

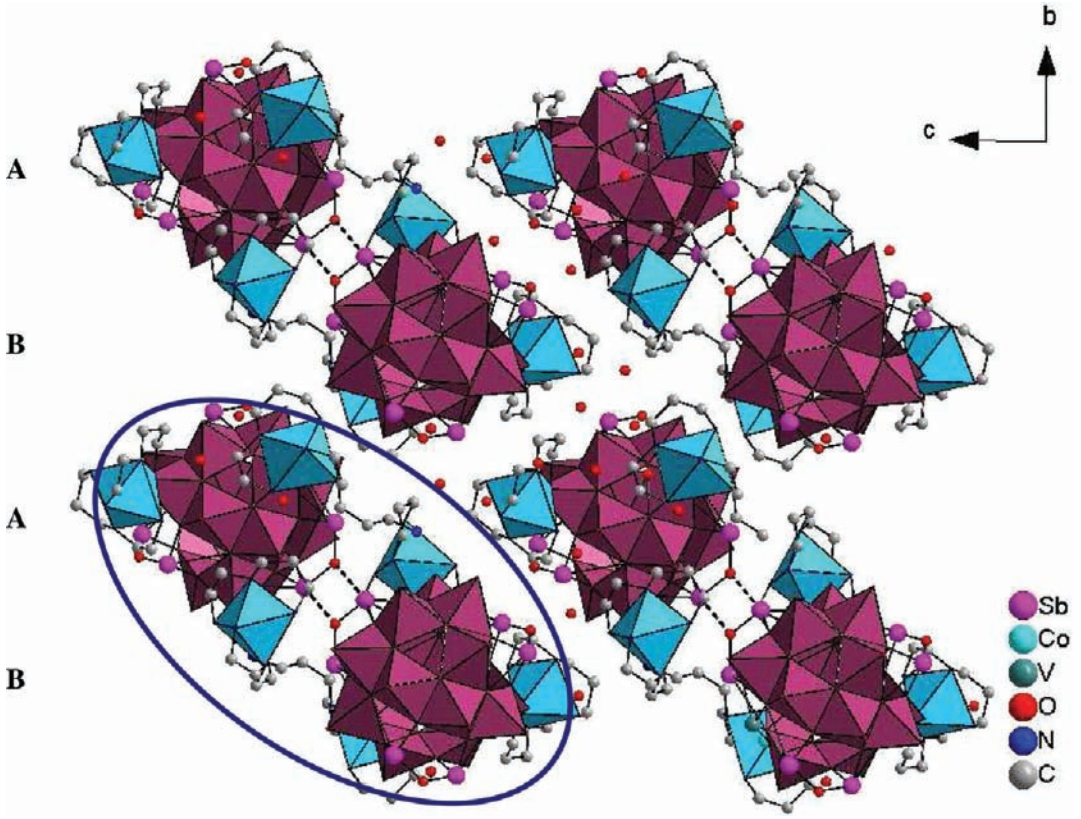

Figure 3. Representation of the cluster pairs in compound **1** in the *bc* plane. A cluster pair is highlighted in the ellipsoidal area. H atoms are omitted for clarity.

dx.doi.org/10.1021/ic2023117 | *Inorg. Chem.* 2012, 51, 2311−2317

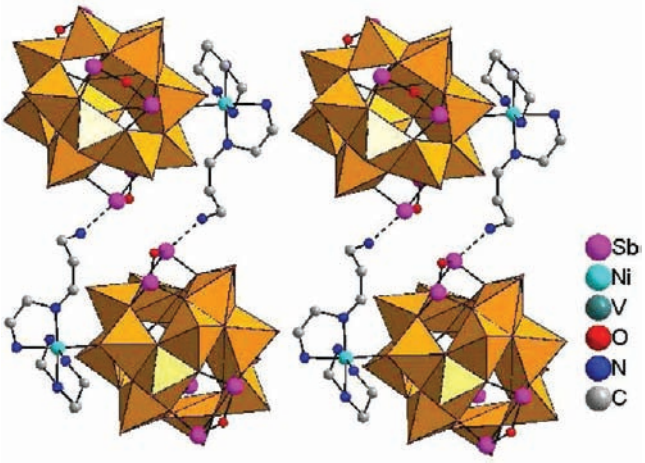

Figure 4. "Rings" in the structure of **2** formed by weak Sb−N interactions. H atoms are omitted for clarity.

interactions. Three clusters and one water molecule are interconnected by every complex cation.

Like in compound **1**, the anionic clusters in compound **2** are arranged in a layer like fashion parallel to the (100) plane with water molecules and the complex cations being located between these layers. Additionally the layers alternate in an ABAB fashion along the *b* axis (Figure 5). The shortest Sb−O separation between adjacent clusters is 3.538(4) Å and thus considerably longer than in compound **1**.

Bond-valence sum (BVS) calculations show that the oxidation state of all the vanadium atoms in the studied compounds is around +4 ($\sum$s = 4.07−4.17 for **1** and $\sum$s = 4.00−4.10 for **2**), which is consistent with the overall charge balance in the formula of both compounds. This is also confirmed by IR spectra of the compounds where the typical vanadyl stretch vibration ν_s(V═O) occurs as a very strong symmetric band at 967 cm^{-1} (Figure 6).

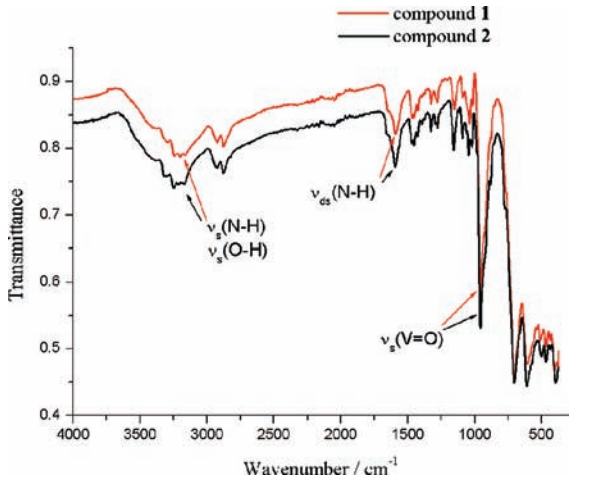

Figure 6. IR spectra of $(Co(N_3C_5H_{15})_2)_2[\{Co(N_3C_5H_{15})_2\}V_{15}Sb_6O_{42}(H_2O)]\cdot 5H_2O$ (**1**) and $(Ni(N_3C_5H_{15})_2)_2[\{Ni(N_3C_5H_{15})_2\}V_{15}Sb_6O_{42}(H_2O)]\cdot 8H_2O$ (**2**). Some prominent bands are labeled.

The BVS calculation for the Sb atoms yields values between 3.42 and 3.59 in **1** and 3.30 and 3.55 in **2**. These values agree with those calculated for Sb atoms in the two compounds $[V^{IV}{}_{14}Sb^{III}{}_8(C_6H_{15}N_3)_4O_{42}(H_2O)]\cdot 4H_2O$ and $(C_6H_{17}N_3)_2[V^{IV}{}_{15}Sb^{III}{}_6(C_6H_{15}N_3)_2O_{42}(H_2O)]\cdot 2.5H_2O$, where also Sb−N interactions were observed.[29]

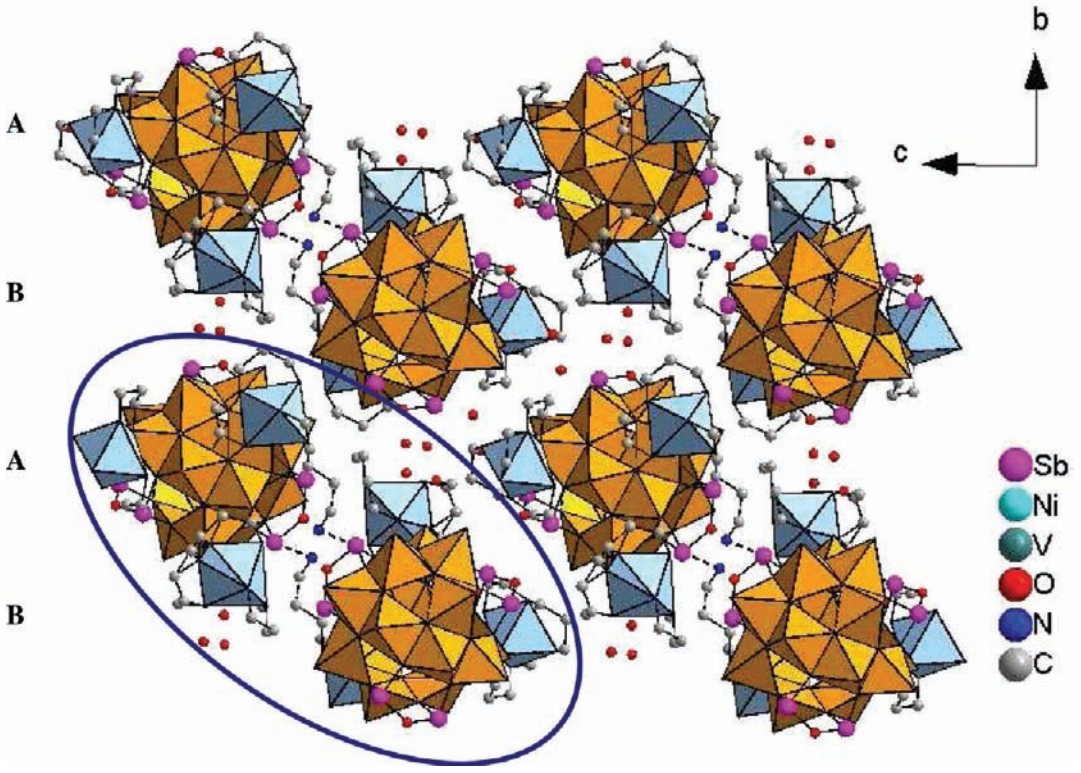

Figure 5. Arrangement of the constituent in the structure of **2** in the *bc* plane. One pair of clusters is marked with the ellipsoidal area. H atoms are omitted for clarity.

dx.doi.org/10.1021/ic2023117 | *Inorg. Chem.* 2012, 51, 2311−2317

The noncoordinated propylamine units in both compounds exhibit different torsion angles (167.984 (9)° for **1** and 77.432 (27)° for **2**) (Figure 7). This leads up to the short Sb−O distance (3.134(3) Å) in **1** and relative short Sb−N interactions (2.654(5) Å) in **2**.

Figure 7. Propylamine moiety of the transition metal complexes and the Sb_2O_5 unit of cluster with an Sb−N distance of 4.4101(2) Å (left) in **1** and 2.6557(3) Å in **2** (right). H atoms are omitted for clarity.

The vibrations ν(O−H) = 3427 (s), ν(H−O−H) = 1596 (s), ν(N−H) = 3250 (s), and ν(C−H) = 2926, 2875 (m) cm^{-1} can be observed in the IR spectrum. The asymmetric ν_{as}(V−O−V) mode appear at 726 cm^{-1}. The characteristic terminal ν_s(V═O) stretching vibration is seen at 967 cm^{-1}. The assignment of the vibrational modes is in accordance with literature data.[40]

Thermal stability [thermogravimetric and differential thermal analysis (TGA/DTA)] measurements in an Ar atmosphere between 20 and 900 °C show almost a continuous decomposition of compound **1** with a total mass loss of Δm_{exp} = 48.3% without well developed decomposition steps (Supporting Information, Figure S1). Nevertheless, two regions in the TG curve can be tentatively distinguished. The first event starts at around 50 °C and proceeds until about 300 °C. Above this temperature further weight loss is observed, and the thermal decomposition reaction is not finished even at 900 °C.

Compound **2** decomposes in at least two steps with a total mass loss of Δm_{exp} = 40.2% (Supporting Information, Figure S2). The first event covers a large temperature range from about 40 to 300 °C (Δm_{exp} = 5.2%) because of loss of water molecules. A complex decomposition behavior is observed above 260 °C with endothermic events at T_p = 356 and 379 °C. In contrast to compound **1**, the stepwise decomposition is more pronounced and during the first step the water molecules are emitted. Above about 260 °C the emission of amine molecules leads to the destruction of the compound. The reflections in the X-ray powder patterns of the black crystalline powders obtained after the thermal decomposition reactions could not be unambiguously assigned.

In a second experiment compound **2** was heated to 200 °C to examine whether water emission leaves the structure intact. The CHN analysis of the sample reveals only a very small loss of organic components (initial: C 11.3; H 3.0; N 7.3%, after thermal treatment up to 200 °C: C 10.3; H 2.7; N 7.1%). In the powder pattern of this product intense reflections can be observed between 2θ = 6.5 and 8.5° which are also present in the pristine compound **2**. All reflections exhibit a shift to either lower scattering angles ((011) and (101)) or higher 2θ values ((−101)), while the (100) reflection is only slightly affected (Figure 8). The heat treatment is accompanied by removal of water leading to an expansion and contraction of the structure in different directions. After treating the sample in water atmosphere the (−101) reflection shifts back to the starting position, whereas (011) shows no significant variation upon water uptake. Interestingly, the (101) reflections exhibits a further shift to smaller scattering angle, that is, the structure expands in this direction (Figure 8). The (−101) layer hosts water molecules and transition metal complexes (Figure 9). The shift of the (−101) peak indicates a reduction of the

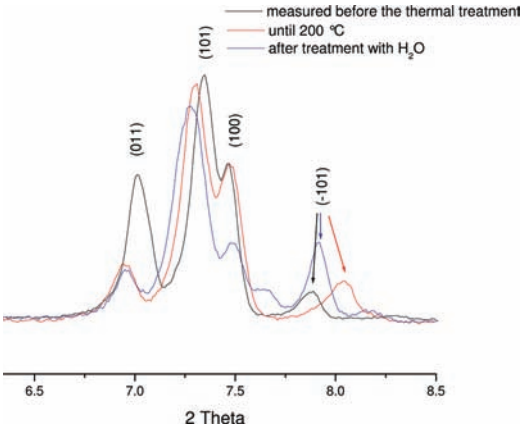

Figure 8. X-ray powder patterns of compound **2** in the 2θ range 6.5−8.5 after different treatments.

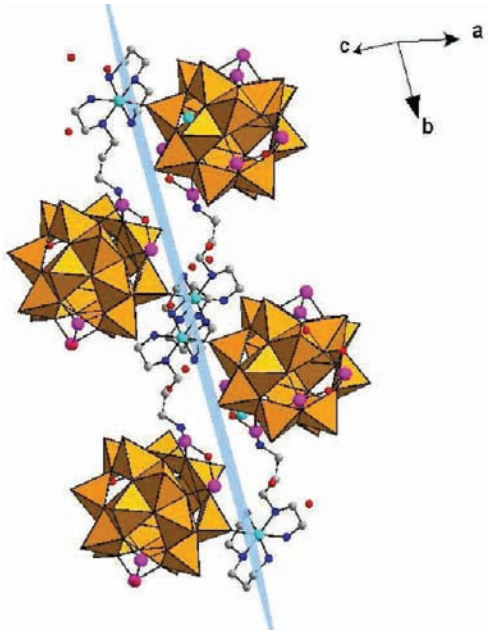

Figure 9. Arrangement of the clusters in compound **2** with the (−101) plane marked light blue. H atoms are omitted for clarity.

distance between the clusters. Unfortunately, the quality of selected single crystals heated at different temperatures was too low for single crystal structure analysis.

The low-field susceptibility data for **1** and **2** indicates that both the two $[M^{II}(N_3C_5H_{15})_2]^{2+}$ countercations as well as the coordinated $\{M^{II}(N_3C_5H_{15})_2\}$ groups do not significantly couple with the S = 1/2 vanadyl groups of the $\{V_{15}Sb_6\}$ core structure. The resulting temperature-dependent $\chi_{mol}T$ data sets thus can be decomposed into the additive single-ion contributions of the three M(II) complexes (per formula unit) and the contribution of the $\{V_{15}Sb_6\}$ group displaying a distinct shoulder plateau around 15−50 K which stems from the geometric spin frustration of its central three vanadyl groups forming a regular triangle (Figure 10). Note that the accurate simulation of the single-ion susceptibility of the octahedral Co^{2+} and Ni^{2+} complexes mandates to take into account their ligand field effects and spin−orbit coupling. Using our simulational framework CONDON 2.0,[41] the susceptibility data for **1** could only be reproduced for the assumption of a distorted (D_{4h} vs O_h) ligand field for the three Co(II) spin

dx.doi.org/10.1021/ic2023117 | Inorg. Chem. 2012, 51, 2311−2317

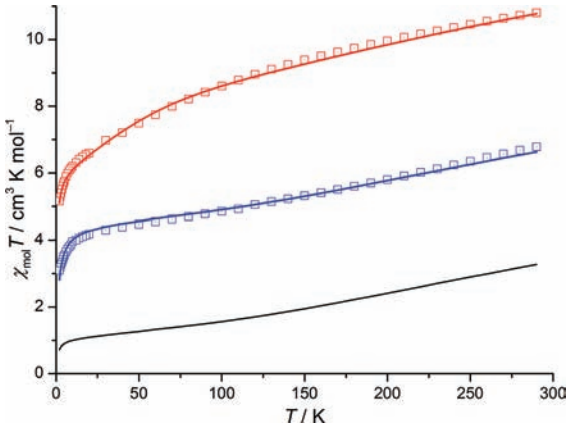

Figure 10. Temperature dependence of $\chi_{mol}T$ of **1** (blue squares) and **2** (red squares) at a static external field of 0.1 T. The blue and red graphs represent the additive contributions of the $\{V_{15}Sb_6\}$ polyanion (black graph, see ref 15) and the three (uncoupled) $[M^{II}(N_3C_5H_{15})_2]^{2+}$ groups, taking their single-ion effects into account.

centers, whereas an O_h-symmetric Ni(II) ligand field proved adequate to reproduce the data for **2**, in line with the observed geometric distortion of the MN_5O and MN_6 octahedra. Using standard spectroscopic data, a least-squares fit was obtained for the ligand field parameters (in Wyborne notation) $B^2_0 = -330$ cm^{-1}, $B^4_0 = 33150$ cm^{-1}, and $B^4_4 = 19631$ cm^{-1} for **1** and $B^4_0 = 39780$ cm^{-1} for **2** (uniformly adapted for all three $[M^{II}(N_3C_5H_{15})_2]^{2+}$ groups; for the definition of the corresponding Hamiltonian see ref 39). Note that such a scenario of a $\{V_{15}E_6\}$ cluster (E = As, Sb) in a matrix of different paramagnetic cations can be of great interest for a systematical assessment of the environmental effects of the $\{V_{15}E_6\}$ cluster on its spin coherence.

3. CONCLUSIONS

Applying identical starting material ratios but varying the transition metal and reaction temperature lead to crystallization of compounds **1** and **2**. The structures of the two compounds are characterized by different arrangements of the propylamine ligands around the transition metal cations covalently bound to the spherical $[V_{15}Sb_6O_{42}]^{6-}$ cluster shells thus featuring short intermolecular Sb···O interactions in **1** while in **2** a short Sb···N interaction is realized. The results of the magnetic characterization indicate that the different paramagnetic cations exhibit no significant coupling to the spins of the cluster anions. Nevertheless, the scenario of a $\{V_{15}E_6\}$ cluster in the environment of different paramagnetic cations may allow a systematical study of effects onto the spin decoherence of the $\{V_{15}E_6\}$ cluster anions.

4. EXPERIMENTAL DETAILS

$(Co(N_3C_5H_{15})_2)_2[\{Co(N_3C_5H_{15})_2\}V_{15}Sb_6O_{42}(H_2O)]\cdot 5H_2O$ (**1**): a mixture of 125 mg (1.1 mmol) of NH_4VO_3, 115 mg (0.39 mmol) of Sb_2O_3, and 107 mg (0.45 mmol) of $CoCl_2\cdot 6H_2O$ in a 4 mL 50% solution of *N*-2-aminoethyl-1,3-propanediamine and water was sealed in a 30 mL Teflon lined stainless steel autoclave and heated at 130 °C for 7 days. After cooling to room temperature the product was filtered and washed with water and acetone, and dried in vacuum. The compound **1** consists of brown particles. Elemental analysis of the brown crystals: C 11.7, H 3.4, N 8.4%, calc. for $C_{30}H_{102}Co_3N_{18}O_{48}Sb_6V_{15}$: C 11.4, H 3.3, N 7.99%. Yield: 45% based on antimony.

For $(Ni(N_3C_5H_{15})_2)_2[\{Ni(N_3C_5H_{15})_2\}V_{15}Sb_6O_{42}(H_2O)]\cdot 8H_2O$ (**2**) 125 mg (1.1 mmol) of NH_4VO_3, 115 mg (0.39 mmol) of Sb_2O_3, 107 mg (0.45 mmol) of $NiCl_2\cdot 6H_2O$, and 4 mL of a 50% solution of *N*-2-aminoethyl-1,3-propanediamine and water, were sealed in a Teflon lined stainless steel autoclave. The reaction mixture was kept at 150 °C for 7 days. Compound **2** can also be prepared by replacing $NiCl_2\cdot 6H_2O$ with Ni (elemental) (0.43 mmol), $Ni(NO_3)_2\cdot 6H_2O$ (0.45 mmol), $NiSO_4\cdot 6H_2O$ (0.45 mmol), $Ni(Ac)_2\cdot 4H_2O$ (0.45 mmol) or $Ni(C_5H_7O_2)_2$ (0.276 mmol). Compound **2** as crystalline powder can also be prepared under dynamical conditions at 150 °C in 6 h. Yield 60% based on antimony. The product brown crystals was washed with water and acetone and dried in vacuum. Elemental analysis of brown crystals: C 11.3, H 3.0, N 7.3%, calc. for $C_{30}H_{108}N_{18}Ni_3O_{51}Sb_6V_{15}$: C 11.3, H 3.3, N 7.9%. SEM images of crystals of compounds **1** and **2** are shown in Supporting Information, Figure S3.

4.1. Crystal Structures Determination. The X-ray intensity data of a single crystal of compound **1** with dimension of 0.062 × 0.10 × 0.14 mm^3 and of a crystal of compound **2** with dimension 0.15 × 0.11 × 0.07 mm^3 were collected at room temperature for **1** and at 170 K for **2** using a STOE-1 Imaging Plate Diffraction System (IPDS-1) with Mo−Kα radiation (λ = 0.71073 Å)). The raw intensities were treated in the usual way applying Lorentz polarization as well as absorption correction. Selected crystal data and details of the structure determination are summarized in Table 1. The structure was solved by direct methods with SHELXS-97.[42] Crystal structure refinements were done against F^2 using SHELXL-97.[42] The CH and NH hydrogen atoms were positioned with idealized geometry and refined using a riding model. The H atoms from water were not located. A numerical absorption correction was performed (for compound **1** T_{min}/T_{max} 0.629, 0.784; for compound **2** T_{min}/T_{max} 0.604, 0.763). After structure refinement of compound **2** there were several additional peaks in the electron density map indicating disorder, for which no reasonable structure model can be found. Therefore, the data were corrected for disordered solvent molecules using the SQUEEZE option in Platon.[43] During the squeezing procedure 48 electrons were collected. The residual electrons may be explained with disordered H_2O molecules. Calculation of the accessible free space using the program suite Platon yields 124.2 Å^3 as potential solvent area for **2**. For **1** the CALC VOID option in Platon was used to calculate Percent Filled Space, which amounts to 75.7%. Comparisons of the powder X-ray diffraction patterns of both compounds simulated from single crystal data with experimental patterns are shown in the Supporting Information, Figure S4 and S5, demonstrating phase purity of the samples.

Crystallographic data of both compounds have been deposited in the Cambridge Crystallographic Data Centre as supplementary publication no CCDC 855593 and 855594.

4.2. Elemental Analysis. CHN analyses were done using a EURO EA Elemental Analyzer.

4.3. IR Spectroscopy. IR spectroscopy measurements (4000−400 cm^{-1}) were performed at room temperature using a Bruker Alpha P FT-IR spectrometer.

4.4. Thermal Analysis. The DTA/TG investigations were carried out in an argon flow (purity: 4.6; heating rate: 4 K/min; flow rate: 75 mL/min; Al_2O_3 crucibles) using a Netzsch STA-409CD instrument.

4.5. X-ray Powder Patterns. X-ray powder patterns were performed on a STOE STADI P diffractometer with Ge monochromator in transmission mode (Cu $K_{\alpha 1}$ radiation, flat sample holders) operated at 40 kV and 30 mA.

4.6. Magnetic Susceptibility Measurements. Susceptibility data were recorded as a function of temperature (2.0−290 K) and field (0.1−5.0 T) using a Quantum Design MPMS-5XL SQUID magnetometer. The following standard Racah and spin−orbit constants have been employed in the CONDON simulations: B = 825 cm^{-1}, C = 3330 cm^{-1}, ζ = 533 cm^{-1} (**1**) and B = 1084 cm^{-1}, C = 4831 cm^{-1}, ζ = 649 cm^{-1} (**2**).

■ ASSOCIATED CONTENT

Supporting Information

Crystallographic data in CIF format. Further details are given in Tables S1 and S2 and Figures S1−S3. This material is available free of charge via the Internet at http://pubs.acs.org.

■ AUTHOR INFORMATION

Corresponding Author

*E-mail: wbensch@ac.uni-kiel.de. Phone: +49 431 880 2091. Fax: +49 431 880 1520.

■ ACKNOWLEDGMENTS

Financial support by the State of Schleswig-Holstein is gratefully acknowledged.

■ REFERENCES

(1) Pope, M. T.; Müller, A. *Angew. Chem.* **1991**, *103*, 56.
(2) Khan, M. I.; Tabussum, S.; Marshall, C. L.; Neylon, M. K. *Catal. Lett.* **2001**, *112*, 1.
(3) Wittingham, M. S.; Chen, R.; Chirayil, T.; Zavalij, P. Y. *Proc. Electrochem. Soc.* **1996**, *76*, 95.
(4) Pless, J. D.; Ko, D.; Hammond, R. R.; Bardin, B. B.; Stair, P. C.; Poeppelmeier, K. R. *J. Catal.* **2004**, *223*, 419.
(5) (a) Müller, A.; Reuter, H.; Dillinger, S. *Angew. Chem., Int. Ed. Engl.* **1995**, *34*, 2328. (b) Müller, A.; Kögerler, P.; Kuhlmann, C. *Chem. Commun.* **1999**, 1347.
(6) Yamase, T.; Fukaya, K.; Nojiri, H.; Ohshima, Y. *Inorg. Chem.* **2006**, *45*, 7698.
(7) Dolbecq, A.; Compain, J. -D.; Mialane, P.; Marrot, J.; Riviere, E.; Secheresse, F. *Inorg. Chem.* **2008**, *47*, 3371.
(8) Krebs, B.; Droste, E.; Piepenbrink, M.; Vollmer, G. *C. R. Acad. Sci., Ser. IIc: Chim.* **2000**, *3*, 205.
(9) Sazani, G.; Dickman, M. H.; Pope, M. T. *Inorg. Chem.* **2000**, *39*, 939.
(10) Zhang, Q.-B.; Lu, Y.-K.; Liu, Y.-B.; Lu, J.; Bi, M.-H.; Yu, J.-H.; Wang, T.-G.; Xu, J.-Q.; Liu, J. *Inorg. Chem. Commun.* **2006**, *9*, 544.
(11) Khenkin, A. M.; Shimon, L. J. W.; Neumann, R. *Eur. J. Inorg. Chem.* **2001**, 789.
(12) Kortz, U.; Savelieff, M. G.; Ghali, F. Y. A.; Khalil, L. M.; Maalouf, S. A.; Sinno, D. I. *Angew. Chem., Int. Ed.* **2002**, *41*, 4070.
(13) Drewes, D.; Vollmer, G.; Krebs, B. *Z. Anorg. Allg. Chem.* **2004**, *630*, 2573.
(14) Kiebach, R.; Näther, C.; Bensch, W. *Solid State Sci.* **2006**, *8*, 964.
(15) Kiebach, R.; Näther, C.; Kögerler, P.; Bensch, W. *Dalton Trans.* **2007**, 3221.
(16) Wutkowski, A.; Näther, C.; Kögerler, P.; Bensch, W. *Inorg. Chem.* **2008**, *47*, 1916.
(17) Hu, X.-X.; Xu, J. -Q.; Cui, X.-B.; Song, J.-F.; Wang, T.-G. *Inorg. Chem. Commun.* **2004**, *7*, 264.
(18) Zhang, L.; Zhao, X.; Xu, P.; Wang, T. *J. Chem. Soc., Dalton Trans.* **2002**, 3275.
(19) Albonetti, S.; Cavani, F.; Trifiro, F.; Gazzano, M.; Aissi, F. C.; Aboukais, A.; Guelton, M. J. *J. Catal.* **1994**, *146*, 491.
(20) Cavani, F.; Tanguy, A.; Trifiro, F.; Koutrev, M. *J. Catal.* **1998**, *174*, 231.
(21) Sprengler, J.; Anderle, F.; Bosch, E.; Grasselli, R. K.; Pillep, B.; Behrens, P.; Lapina, O. P.; Shubin, A. A.; Eberle, H.-J.; Knözinger, H. *J. Phys. Chem. B* **2001**, *105*, 10772.
(22) Do, J.; Jacobson, A. J. *Inorg. Chem.* **2001**, *40*, 2468.
(23) Wutkowski, A.; Näther, C.; Speldrich, M.; Kögerler, P.; Bensch, W. *Z. Anorg. Allg. Chem.* **2009**, *635*, 1094.
(24) Li, Y.; Liu, J. P.; Wang, J. P.; Niu, J. Y. *Chem. Res. Chin. Univ.* **2009**, *25*, 426.
(25) Gao, Y. Z.; Han, Z. G.; Xu, Y. Q.; Hu, C. W. *J. Clust. Sci.* **2010**, *21*, 163.
(26) Cui, X.-B.; Xu, J.-Q.; Sun, Y. -H.; Li, Y.; Ye, L.; Yang, G.-Y. *Inorg. Chem. Commun.* **2004**, *7*, 58.
(27) Qi, Y.; Li, Y.; Wang, E.; Zhang, Z.; Chang, S. *Dalton Trans.* **2008**, 2335.
(28) Dong, B.-X.; Peng, J.; Gómez-García, C. J.; Benmansour, S.; Jia, H.-Q.; Hu, N.-H. *Inorg. Chem.* **2007**, *46*, 5933.
(29) Zheng, S.-T.; Zhang, J.; Xu, J.-Q.; Yang, G.-Y. *J. Solid State Chem.* **2005**, *178*, 3740.
(30) Zheng, S.-T.; Wang, M.-H.; Yang, G.-Y. *Inorg. Chem.* **2007**, *46*, 9503.
(31) Antonova, E.; Näther, C.; Kögerler, P.; Bensch, W. *Angew. Chem.* **2011**, *123*, 790.
(32) Chiorescu, I.; Wernsdorfer, W.; Müller, A.; Miyashita, S.; Barbara, B. *Phys. Rev. B* **2003**, *67*, 020402.
(33) Procissi, D.; Lascialfari, A.; Micotti, E.; Bertassi, M.; Carretta, P.; Furukawa, Y.; Kögerler, P. *Phys. Rev. B* **2006**, *73*, 184417.
(34) Chaboussant, G.; Ochsenbein, S. T.; Sieber, A.; Güdel, H.-U.; Mutka, H.; Müller, A.; Barbara, B. *Europhys. Lett.* **2004**, *66*, 423.
(35) Chaboussant, G.; Basler, R.; Sieber, A.; Ochsenbein, S. T.; Desmedt, A.; Lechner, R. E.; Telling, M. T. F.; Kögerler, P.; Müller, A.; Güdel, H.-U. *Europhys. Lett.* **2002**, *59*, 291.
(36) Bertaina, S.; Gambarelli, S.; Mitra, T.; Tsukerblat, B.; Müller, A.; Barbara, B. *Nature* **2008**, *453*, 203.
(37) Poisot, M.; Näther, C.; Bensch, W. *Acta Crystallogr.* **2006**, *E62*, m1326.
(38) Ellermeier, J.; Stähler, R.; Bensch, W. *Acta Crystallogr.* **2002**, *C58*, m70.
(39) Zhao, J.-W.; Zheng, S.-T.; Yang, G.-Y. *J. Solid State Chem.* **2007**, *180*, 3317.
(40) Botto, I. L.; Baran, E. J.; Aymonino, P. J. *Monatsh. Chem.* **1976**, *107*, 1127.
(41) Speldrich, M.; Schilder, H.; Lueken, H.; Kögerler, P. *Isr. J. Chem.* **2011**, *51*, 215.
(42) Sheldrick, G. M. *Acta Crystallogr.* **2008**, *A64*, 112.
(43) Spek, A. L. *PLATON, A multipurpose crystallographic tool*; Utrecht University: Utrecht, The Netherlands, 2000.